Electric-Field Control of Nonvolatile Magnetization in $Co_{40}Fe_{40}B_{20}/Pb(Mg_{1/3}Nb_{2/3})_{0.7}Ti_{0.3}O_3$ Structure at Room Temperature

S. Zhang,[1] Y. G. Zhao,[1,*] P. S. Li,[1] J. J. Yang,[1] S. Rizwan,[2] J. X. Zhang,[3,8] J. Seidel,[3] T. L. Qu,[1,3] Y. J. Yang,[4] Z. L. Luo,[4] Q. He,[3] T. Zou,[2] Q. P. Chen,[1] J. W. Wang,[1] L. F. Yang,[1] Y. Sun,[2] Y. Z. Wu,[6] X. Xiao,[6] X. F. Jin,[6] J. Huang,[7] C. Gao,[4,5] X. F. Han,[2] and R. Ramesh[3]

[1]*Department of Physics and State Key Laboratory of Low-Dimensional Quantum Physics, Tsinghua University, Beijing 100084, China*
[2]*Beijing National Laboratory for Condensed Matter Physics, Chinese Academy of Sciences, Beijing 100190, China*
[3]*Department of Materials Science and Engineering, University of California, Berkeley, California 94720, USA*
[4]*National Synchrotron Radiation Laboratory, University of Science and Technology of China, Hefei, Anhui 230026, China*
[5]*Department of Materials Science and Engineering, University of Science and Technology of China, Hefei, Anhui 230026, China*
[6]*Department of Physics, State Key Laboratory of Surface Physics and Advanced Materials Laboratory, Fudan University, Shanghai 200433, China*
[7]*Bruker Nano Surfaces Business, Beijing 100081, China*
[8]*Beijing Normal University, Department of Physics, Beijing 100875, China*

(Received 10 September 2011; published 28 March 2012)

We report a large and nonvolatile bipolar-electric-field-controlled magnetization at room temperature in a $Co_{40}Fe_{40}B_{20}/Pb(Mg_{1/3}Nb_{2/3})_{0.7}Ti_{0.3}O_3$ structure, which exhibits an electric-field-controlled *looplike* magnetization. Investigations on the ferroelectric domains and crystal structures with *in situ* electric fields reveal that the effect is related to the combined action of 109° ferroelastic domain switching and the absence of magnetocrystalline anisotropy in $Co_{40}Fe_{40}B_{20}$. This work provides a route to realize large and nonvolatile magnetoelectric coupling at room temperature and is significant for applications.

DOI: 10.1103/PhysRevLett.108.137203 PACS numbers: 75.80.+q, 77.65.−j, 75.85.+t

With the fast development of information storage, exploiting new concepts for dense, fast, and nonvolatile random access memory with reduced energy consumption is a significant and challenging task. To realize this goal, electric-field control of magnetism is crucial [1–3]. A promising way to control magnetism via electric fields is using the converse magnetoelectric (ME) effect [2], which permits control of magnetism with electric fields rather than with electric currents or with magnetic fields [3]. In that context, multiferroic materials which exhibit simultaneous magnetic and ferroelectric orders with coupling between them are among the top candidates for realizing electric-field control of magnetism [4–6]. However, single-phase multiferroic materials are rare at room temperature and the converse ME effects are typically also too small to be useful [2]. The use of artificial two-phase systems consisting of ferromagnetic (FM) and ferroelectric (FE) materials, especially various room temperature FM and FE materials, serves as an alternative approach to achieve electric-field control of magnetism and has been widely studied in recent years [2,7–12].

For the electric-field control of magnetism, tunable and nonvolatile converse ME effects are two important requirements for information storage. In the strain-mediated FM-FE two-phase system, the bipolar-electric-field-controlled magnetization generally exhibits a reversible, *butterflylike* behavior [7–11] and the understanding of it has been well established in terms of the piezostrain of the FE substrate transferred to the FM layer. In this case, the change of magnetization is volatile because the piezostrain vanishes when the driving electric field is removed. Some exceptions have been reported, e.g., in $La_{0.67}Sr_{0.33}MnO_3/BaTiO_3$ FM-FE heterostructures, an electric-field-controlled nonvolatile converse ME effect was present [2]. However, in this case both positive and negative electric fields can only change the sample from a large magnetization to a small one and a series of complicated processes is needed to reset the large magnetization rather than to simply change the electric field. It was also reported that the electric-field induced remanent strain or irreversible ferroelectric domain effect controls the magnetization [8,12]; however, a specific value or range of electric field is required to induce the effect in these systems and the magnetization controlled by electric fields shows obvious relaxation with time [8], which are disadvantageous for applications. Therefore, in the FM-FE two-phase system, a tunable and nonvolatile converse ME effect at room temperature is highly desired.

$Co_{40}Fe_{40}B_{20}$ (CoFeB) belongs to the class of amorphous ferromagnetic Co-Fe-B alloys, which shows perfect soft ferromagnetism [13] without magnetocrystalline anisotropy and possesses the highest spin polarization among Co-Fe-B compounds [14] giving rise to a large tunneling magnetoresistance (TMR) in magnetic tunnel junctions [15]. Considering the absence of magnetocrystalline anisotropy and the low coercive field, it is interesting to explore the electric-field control of magnetism of CoFeB thin film in FM-FE structures. Moreover, the electric-field

control of magnetism in these kinds of materials is also a key approach for electric-field-controlled TMR, which has been proposed theoretically as a way to achieve electric-write nonvolatile memory [16].

In this Letter, we report a large, tunable and nonvolatile converse ME effect at room temperature in a FM-FE structure composed of CoFeB and $Pb(Mg_{1/3}Nb_{2/3})_{0.7}Ti_{0.3}O_3$ (PMN-PT). The magnetization of CoFeB film exhibits a *looplike* response to electric field instead of the *butterflylike* behavior commonly observed in the piezostrain-mediated FM-FE structures [7–11]. Through systematic investigation of the ferroelectric domains and crystal structures using piezoresponse force microscopy (PFM) and high-resolution x-ray reciprocal space mapping (RSM) with *in situ* electric fields, it was demonstrated that the *looplike* magnetization response to the electric field originates from the combined action of 109° ferroelastic domain switching in PMN-PT and the absence of magnetocrystalline anisotropy in CoFeB.

Heterostructures composed of amorphous CoFeB film and PMN-PT substrate were prepared by magnetron sputtering and the properties of the samples were measured by various techniques. Sample configuration is shown in Fig. 1(a) and the detailed experimental methods are presented in the Supplemental Material [17]. The magnetic hysteresis loops were measured along the [110] direction under electric fields of 0 $kV\,cm^{-1}$, ± 1 $kV\,cm^{-1}$, and ± 8 $kV\,cm^{-1}$, respectively, and the maximum change in magnetization occurs between $+8$ $kV\,cm^{-1}$ and -8 $kV\,cm^{-1}$, which are shown in Fig. 1(b). It can be seen that positive electric fields tend to decrease the magnetization, while negative electric fields tend to increase it. It also reveals that the converse ME effect is more remarkable at low magnetic fields. To explore the correlation between the change of magnetization and electric field directly, we measured the variation of magnetization along the [110] direction with the electric field at 5 Oe. The polarization current was also obtained at the same time. The variation of magnetization with the electric field guided by the dashed arrows is shown in Fig. 1(c), which turns out to be a *looplike* magnetization-electric field response and the magnetization changes sharply with the polarization switching process in PMN-PT as revealed by the polarization current peak. Thus, the magnetization-electric field curve for our CoFeB/PMN-PT FM-FE structure is clearly distinct from previous reports on magnetization-electric field curves of piezostrain-mediated FM-FE structures [7–11], which exhibit *butterflylike* magnetization-electric field curves and the change of magnetization is volatile. Although *looplike* magnetization-electric field curves have been reported in $La_{0.8}Sr_{0.2}MnO_3$/FE [18] and dilute magnetic semiconducting $Ga_{1-x}Mn_xAs$/FE [19], the effect in their systems occurs below 100 K and the mechanisms are different from the present work as mentioned later. Thus, the large, tunable and nonvolatile converse ME effect reported here is particularly important in terms of room temperature applications involving electric-field control of magnetism. Since the magnetization of CoFeB can be tuned by bipolar electric fields and is nonvolatile as shown in Fig. 1(c), stable and remarkable high/low magnetization states can be achieved by switching the polarity of electric field as shown in Fig. 1(d). Similar measurements were carried out along the [− 110] direction, and the results (Fig. S1 of [17]) show a reverse behavior compared to those of the [110] direction (Fig. 1). The magnetoelectric coefficient ($\alpha = \mu_0 dM/dE$) accompanying the polarization switching is nearly 2×10^{-6} $s\,m^{-1}$ (Fig. S1(c) of [17]), which is about 1 or 2 orders of magnitude larger than the previous reports [2,7,9]. The fatigue and retention properties of the ME effect have also been investigated (Fig. S1(e) and S1(f) of [17]), which further demonstrated the tunability and nonvolatility of the electric-field-controlled magnetization.

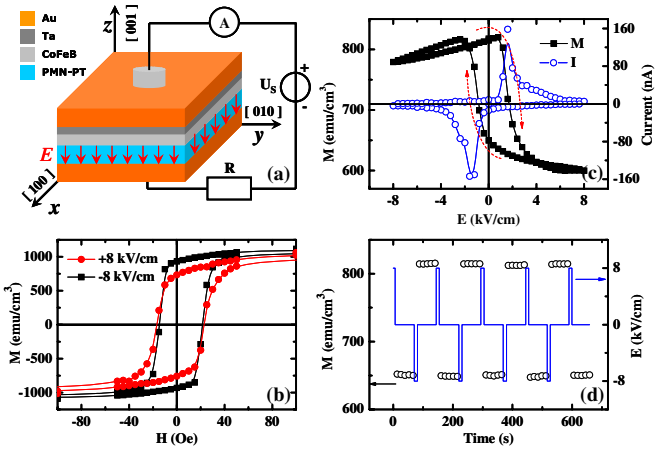

FIG. 1 (color online). (a) Scheme of the sample and experimental configuration. (b) In-plane magnetic hysteresis loops under electric fields of $+8$ $kV\,cm^{-1}$ (circle) and -8 $kV\,cm^{-1}$ (square). (c) Electric-field tuning of the in-plane magnetization (square) and polarization current (open circle) recorded at the same time. (d) The repeatable high/low magnetization states (open circle) switched by pulsed electric fields (blue line).

To understand the electric-field control of magnetism in our CoFeB/PMN-PT structure, the effect of electric field on the magnetic anisotropy of CoFeB was explored by using electron spin resonance (Fig. S2 of [17]). It shows that the as-grown CoFeB film exhibits an in-plane magnetic isotropy. After poling, it changes to a uniaxial magnetic anisotropy with the easy and hard directions of magnetization along [110] and [− 110], respectively. The direction of the uniaxial magnetic anisotropy does not change with the polarity of electric field; however, a positive electric field leads to a weaker uniaxial anisotropy compared to the negative electric field of the same amplitude. This can account for the experimental observation that a positive electric field decreases the magnetization of CoFeB along [110] and increases the magnetization along [− 110], while a negative electric field does the opposite. Comparing the magnetization-electric field curves with the corresponding polarization current curves (Fig. 1(c) and

also S1(b) of [17]), one can deduce that the nonvolatile ME effect is associated with the FE domain switching in PMN-PT. However, it should be pointed out that our results cannot be explained by the scenario related to the electric-field induced charge accumulation/dissipation at the interface [18] or a surface effect due to the polarization switching in the ferroelectric layer [20], because the contributions from these two scenarios are too small to account for the observed large change in magnetization which should originate from the whole film.

The composition of PMN-PT used in our work is in the region of the morphotropic phase boundary [21], which possess not only an ultrahigh piezoelectric response [22] but also complicated phase structures and ferroelectric domains [23–25]. One of the major structures of PMN-PT is the rhombohedral phase with spontaneous ferroelectric polarizations along ⟨111⟩ directions (the body diagonals of the pseudocubic unit cell) at room temperature [21] as in rhombohedral $BiFeO_3$, and there are eight equivalent polarization directions, which can be switched by 71°, 109° and 180°, respectively [26]. As a powerful technique for directly observing the FE domains and switching category, PFM was used to investigate the ferroelectric domain state and polarization switching in the PMN-PT with the cantilever along the [110] direction. Figures 2(a) and 2(b) are the PFM images of the unpoled PMN-PT for the out-of-plane and in-plane cases, respectively. Based on the piezoresponse analysis [27], the polarization directions can be deduced as shown in Fig. 2(c), which agrees with the nature of the rhombohedral structure. After poling a 5 μm by 5 μm square in the center of a 10 μm by 10 μm visual field with a -12 V dc voltage biased by the tip, the color of the out-of-plane image becomes black [Fig. 2(d)] in the poled area and the color of the in-plane one changes to brown [Fig. 2(e)], which means that all the out-of-plane polarization components are switched upward and the in-plane ones mainly have two possible directions, nominally [111] and [− 1 − 11] as shown in Fig. 2(f). The reduction of polarization directions was also observed in the poled PMN-PT single crystals [25] and explained by considering the strain compatibility criteria and the weak random field. In the case of +12 V bias voltage, the out-of-plane image becomes white [Fig. 2(g)], representing the out-of-plane polarization components switched downward as shown in Fig. 2(i), while for the in-plane image shown in Fig. 2(h) some white regions appear inside the brown area, as marked by the red circle and dashed bars. We can deduce the in-plane polarization directions as shown in Fig. 2(i). Therefore, the white regions correspond to 109° ferroelastic switching [28], while the brown regions are related to 71° or 180° (71/180° for short) switching. The difference between FE domain structures under positive and negative electric fields was also observed in rhombohedral $BiFeO_3$ [29], and can be understood in terms of the internal field induced by impurity doping [30] or point defects of the crystal [31]. Furthermore, besides the dominant [111] and [− 1 − 11] oriented domains at −12 V, there are still some

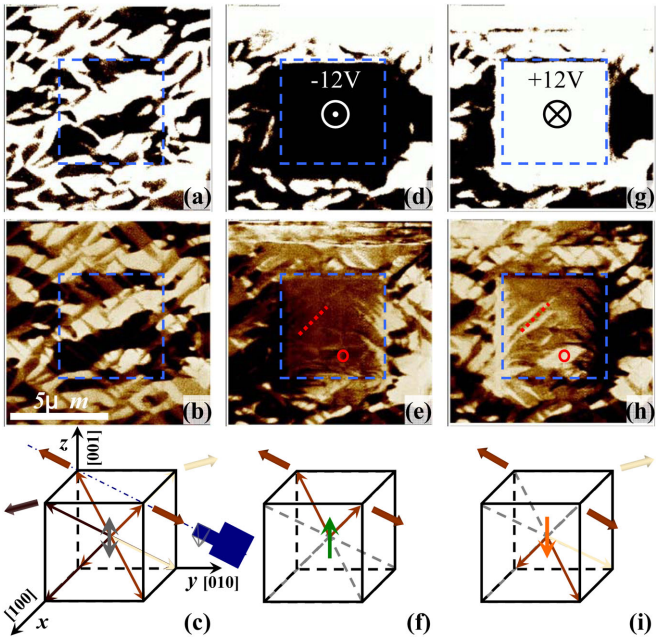

FIG. 2 (color online). (a), (d), and (g) are the out-of-plane phase PFM images while (b), (e), and (h) are the in-plane ones. Corresponding to PFM images in the upper panel, the sketch maps (c), (f), and (i) show the different configurations of the polarization vector under different voltages, where the long arrows along the body diagonals represent the spontaneous polarization vectors in the rhombohedral phase and short arrows in the center of cubic represent the out-of-plane polarization components, respectively. The broad arrows along the diagonals of the top square stand for the in-plane polarization components and their colors correspond to those in the in-plane PFM images (b), (e), and (h).

[− 111] oriented domains and their changes are discussed in Sect. S4 of [17].

PFM probes local regions (micrometer size) rather than the whole area of the sample (millimeter size). In contrast, the x-ray diffraction reciprocal space mapping [32] (XRD-RSM) with the ability to reflect the fraction of rhombohedral distortion for the whole sample [28] is more straightforward. Synchrotron radiation high-resolution XRD-RSM was used with *in situ* electric fields to investigate the change of crystal structure, lattice parameters, and the fractions of different rhombohedral distortions accompanying ferroelectric domain switching. The reflections around the (113) peak under electric fields of $-8\ \mathrm{kV\,cm^{-1}}$, $-0\ \mathrm{kV\,cm^{-1}}$, $+8\ \mathrm{kV\,cm^{-1}}$, and $+0\ \mathrm{kV\,cm^{-1}}$ are shown in Figs. 3(a)–3(d). Interestingly, the overall features of the reflections are almost unchanged after removing the electric field [compare Fig. 3(a) with Fig. 3(b) and compare Fig. 3(c) with Fig. 3(d)], while they show a remarkable difference for the positively and negatively poled cases. This behavior is consistent with the nonvolatile electric-field control of magnetism (Fig. 1 and Fig. S1 of [17]). The configuration of the XRD-RSM measurement around the (113) reflection and the eight possible polarization orientations in the pseudocubic unit

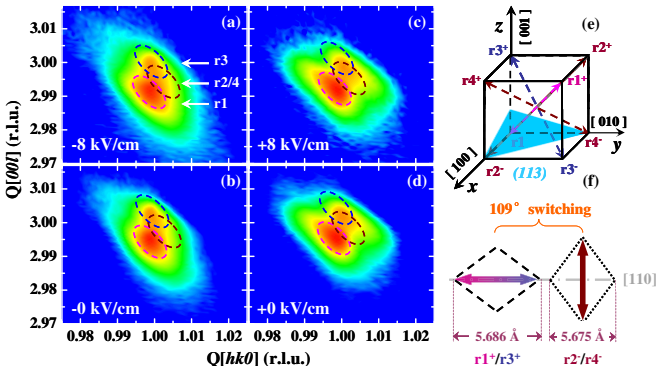

FIG. 3 (color online). (a) to (d) show the electric-field tuned XRD-RSMs around the (113) reflection. Ellipses with different colors in the RSMs draw the outlines of the deduced spots with center positions listed in Table S1. (e) Configuration of the (113) crystal face (translucent blue plane) and the rhombohedral distortions as well as polarizations shown by the arrows, whose colors correspond to the colors of the ellipses in (a) to (d). (f) The 109° switching induced changes of in-plane distortions along the [110] direction as well as the corresponding lattice parameters and the in-plane projections of polarization vectors (broad arrows).

cell of PMN-PT are shown in Fig. 3(e), from which we can deduce the switching category from the changes between different rhombohedral distortions. According to the lattice parameters of the rhombohedral distortion [23] and reported RSM analyzing method [28], we have obtained the position and intensity of spots in the (113) reflection, corresponding to all the possible rhombohedral distortions as well as polarizations (Sect. S5 of [17]). From this analysis, the percentage of $r2/r4$ between the negatively and positively poled cases changes from about 4% to 30%, which is consistent with the remarkable difference of intensity distribution of the RSM results shown in Fig. 3, and also the direct PFM observation shown in Fig. 2. Since the change between $r1^{+}/r3^{+}$ and $r2^{-}/r4^{-}$ corresponds to the 109° switching [Fig. 3(f)], therefore the percentage of 109° switching is about 26% and the 71/180° switchings share the balance of 74%. It should be noticed that the amount of 109° switching is consistent with the relative change of magnetization (see discussion in Sect. S5 of [17]), suggesting their correlation. Quantitative analysis on the position variation of the obviously changed spots in all the RSMs around the (113) reflection was carried out (Sect. S6 of [17]), and the electric-field dependence of the lattice parameter and corresponding strain along the [110] direction exhibits a giant *looplike* behavior (ferroelastic strain) as shown in Fig. S3(j) of [17], consistent with the magnetization-electric field curves [Fig. 1(c)].

The aforementioned results can be understood as follows. The as-grown CoFeB on the unpoled PMN-PT substrate shows an in-plane magnetic isotropy due to its amorphous nature and the randomness of ferroelectric domains. After negative poling, most of the ferroelectric domains align in the [110] direction [see Fig. 2(f) and also the quantitative RSM results listed in Table S2] to reduce the ferroelastic energy, leading to a longer distortion along the [110] direction. This induces a uniaxial magnetic anisotropy in the CoFeB layer with the easy direction of magnetization along [110] and hard direction along [− 110] (Fig. S2(b) of [17]). For the positive poling, some ferroelectric domains switch by 109° while others switch by 71/180° as shown in Fig. 2(i) with fractions listed in Table S2. In contrast to the 71/180° switching, the 109° switching (e.g., switching from $r1^{+}/r3^{+}$ to $r2^{-}/r4^{-}$ under electric fields changing from negative to positive) changes the elongated distortions from the [110] direction for negative poling to the [− 110] direction for positive poling (see Fig. 3(f) and detailed scheme in Fig. S4 of [17]), resulting in complementary ferroelastic strains along the [110] and [− 110] directions with a *looplike* behavior for the strain-electric field curve (Fig. S3(j) of [17]), which is consistent with the *looplike* magnetization-electric field curves and the complementary behavior for the [110] and [− 110] directions [Fig. 1(c) and Fig. S1(b)]. It should be emphasized, besides 109° switching in PMN-PT, the absence of magnetocrystalline anisotropy in amorphous CoFeB is also important, which makes the magnetization sensitive to the ferroelastic strain related to the 109° domain switching. In the previous reports [7,9], the effective magnetic field related to the magnetocrystalline anisotropy suppresses the response of magnetization to the ferroelastic strain related to the 109° domain switching, resulting in the *butterflylike* magnetization-electric field curve with a much smaller change in magnetization. A similar ME effect, as reported here, should be expected for FM/FE structures consisting of nonepitaxial FM layers with weak or no magnetocrystalline anisotropy and FEs with 109° ferroelastic switching. It should be mentioned that our mechanism is different from the previous report [33], which is based on the exchange coupling between $BiFeO_3$ and CoFe.

In summary, large, tunable and nonvolatile electric-field control of magnetization at room temperature and giant magnetoelectric coupling were achieved in CoFeB/PMN-PT. It was demonstrated that the ME effect originates from the direct coupling between the FE domain and FM film with the combined action of 109° ferroelastic domain switching in PMN-PT and the absence of magnetocrystalline anisotropy in CoFeB. This work is significant for exploring novel mechanisms of electric-field control of magnetism and applications, especially electric-field-controlled TMR to achieve electric-controlled magnetic random access memories.

This work was supported by the 973 project of the Ministry of Science and Technology of China (Grants No. 2009CB929202, No. 2009CB929203, No. 2012CB922004, and No. 2010CB934400), National Science Foundation of China (Grants No. 50872065, No. 10721404, No. 11179008, and No. 51021061), and Special Fund of Tsinghua for basic research (Grant No. 201110810625). Tsinghua National Laboratory for

Information Science and Technology (TNList) Cross-discipline Foundation.

*ygzhao@tsinghua.edu.cn

[1] N. A. Spaldin and M. Fiebig, Science **309**, 391 (2005).
[2] W. Eerenstein, M. Wiora, J. L. Prieto, J. F. Scott, and N. D. Mathur, Nature Mater. **6**, 348 (2007).
[3] N. A. Spaldin, S. W. Cheong, and R. Ramesh, Phys. Today **63**, No. 10, 38 (2010).
[4] W. Eerenstein, N. D. Mathur, and J. F. Scott, Nature (London) **442**, 759 (2006).
[5] M. Fiebig, J. Phys. D **38**, R123 (2005).
[6] Y. Tokura, J. Magn. Magn. Mater. **310**, 1145 (2007).
[7] C. Thiele, K. Dörr, O. Bilani, J. Rödel, and L. Schultz, Phys. Rev. B **75**, 054408 (2007).
[8] S. Geprags, A. Brandlmaier, M. Opel, R. Gross, and S. T. B. Goennenwein, Appl. Phys. Lett. **96**, 142509 (2010).
[9] J. J. Yang, Y. G. Zhao, H. F. Tian, L. B. Luo, H. Y. Zhang, Y. J. He, and H. S. Luo, Appl. Phys. Lett. **94**, 212504 (2009).
[10] M. Liu *et al.*, Adv. Funct. Mater. **19**, 1826 (2009).
[11] Y. J. Chen, J. Gao, T. Fitchorov, Z. Cai, K. S. Ziemer, C. Vittoria, and V. G. Harris, Appl. Phys. Lett. **94**, 082504 (2009).
[12] T. Wu, A. Bur, P. Zhao, K. P. Mohanchandra, K. Wong, K. L. Wang, C. S. Lynch, and G. P. Carman, Appl. Phys. Lett. **98**, 012504 (2011).
[13] S. U. Jen, Y. D. Yao, Y. T. Chen, J. M. Wu, C. C. Lee, T. L. Tsai, and Y. C. Chang ,J. Appl. Phys. **99**, 053701 (2006).
[14] T. Kubota, T. Daibou, M. Oogane, Y. Ando, and T. Miyazaki, Jpn. J. Appl. Phys. **46**, L250 (2007).
[15] S. Ikeda, J. Hayakawa, Y. Ashizawa, Y. M. Lee, K. Miura, H. Hasegawa, M. Tsunoda, F. Matsukura, and H. Ohno, Appl. Phys. Lett. **93**, 082508 (2008).
[16] N. A. Pertsev and H. Kohlstedt, Appl. Phys. Lett. **95**, 163503 (2009).
[17] See supplemental material at http://link.aps.org/supplemental/10.1103/PhysRevLett.108.137203.
[18] H. J. A. Molegraaf, J. Hoffman, C. A. F. Vaz, S. Gariglio, D. van der Marel, C. H. Ahn, and J.-M. Triscone, Adv. Mater. **21**, 3470 (2009).
[19] C. Bihler *et al.*, Phys. Rev. B **78**, 045203 (2008).
[20] C. G. Duan J. P. Velev, R. F. Sabirianov, Z. Zhu, J.Chu, S. S. Jaswal, and E. Y. Tsymbal, Phys. Rev. Lett. **101**, 137201 (2008).
[21] S. E. Park and T. R. Shrout, J. Appl. Phys. **82**, 1804 (1997).
[22] H. X. Fu and R. E. Cohen, Nature (London) **403**, 281 (2000).
[23] B. Noheda, D. E. Cox, G. Shirane, J. Gao, and Z.-G. Ye, Phys. Rev. B **66**, 054104 (2002).
[24] F. M. Bai, J. F. Li, and D. Viehland, Appl. Phys. Lett. **85**, 2313 (2004).
[25] A. A. Bokov and Z. G. Ye, J. Appl. Phys. **95**, 6347 (2004).
[26] T. Zhao *et al.*, Nature Mater. **5**, 823 (2006).
[27] F. Zavaliche, S. Y. Yang, T. Zhao, Y. H. Chu, M. P. Cruz, C. B. Eom, and R. Ramesh, Phase Transit. **79**, 991 (2006).
[28] S. H. Baek *et al.*, Nature Mater. **9**, 309 (2010).
[29] Y. H. Chu *et al.*, Adv. Mater. **18**, 2307 (2006).
[30] S. Takahashi, Ferroelectrics **41**, 143 (1982).
[31] V. Gopalan and M. C. Gupta, Appl. Phys. Lett. **68**, 888 (1996).
[32] P. F. Fewster, Crit. Rev. Solid State Mater. Sci. **22**, 69 (1997).
[33] Y. H. Chu *et al.*, Nature Mater. **7**, 478 (2008).